Journal of Polymer Research (2023) 30:456
https://doi.org/10.1007/s10965-023-03834-z

ORIGINAL PAPER

'Spider-like' POSS in NIPU webs: enhanced thermal stability and unique swelling behavior

Izabela Łukaszewska[1] · Artur Bukowczan[1] · Konstantinos N. Raftopoulos[1] · Krzysztof Pielichowski[1]

Received: 27 July 2023 / Accepted: 14 November 2023 / Published online: 2 December 2023

Abstract

PEO-based non-isocyanate polyhydroxyurethane (NIPU, PHU) networks physically modified with octa(3-hydroxy-3-methylbutyldimethylsiloxy)POSS (8OHPOSS) were synthesized via one-pot one-step approach. POSS was introduced into the polymer matrix in the amount of 1–10 wt%. Polar hydroxyls on the vertex groups of POSS allowed for uniform dispersion even up to high loadings (10 wt%). Composites exhibit enhanced thermal stability in comparison to the pristine matrix. FTIR analysis confirmed that POSS strengthens the hydrogen bonding in the material. Upon POSS introduction, plasticization was observed with a peculiar trend change at POSS loadings over 5 wt%. Glass transition temperature of highly crystalline 8OHPOSS was measured and reported to be at around 3 °C. NIPUs at hand exhibit high water absorption (around 200 wt%) typical for hydrogels. Swelling studies show that 8OHPOSS enhances PHUs hydrogels absorption capacity in phosphate-buffered saline (PBS). Higher absorption capacity in PBS solution in comparison to distilled water is an uncommon phenomenon in hydrogels.

Keywords Non-isocyanate polyurethanes · POSS · Hydrogels · Thermal stability · Swelling

Introduction

Non-isocyanate polyurethanes (NIPUs) are a new class of polyurethanes synthesized without isocyanates, which are known to be toxic and environmentally hazardous [1]. The main route for obtaining NIPUs is polyaddition reaction between cyclic carbonates and amines [1, 2], which results in formation of polyhydroxyurethanes (PHUs) with hydroxyl groups close to urethane moieties [3, 4]. The formation of hydroxy-urethane moieties instead of urethanes has a strong impact on the properties of PHUs, e.g. improved water absorption [4–7], increased chemical resistance [8], and enhanced hydrolytic stability [3, 9] in comparison to conventional polyurethanes (PUs).

NIPUs, given their properties and advantages over isocyanate-based PUs, attracted a lot of attention over the last years. PHUs, especially in a form of chemically crosslinked networks, are interesting materials that are suitable for application as hydrogels [7, 10, 11]. Hydrogels include, above all, chemically cross-linked polymers, which, due to their hydrophilic network structure, are able to absorb a mass of water from several to several thousand times greater than their own mass [12, 13]. Polymeric hydrogels are often modified to improve or adjust their properties. The modification usually consists of introducing various additives into the polymer matrix, such as: nucleic acids, proteins, cells, and inorganic nanomaterials (e.g. layered silicates) [14].

One of the most widely studied groups of nanoadditives are polyhedral oligomeric silsesquioxanes (POSS) – organic/inorganic hybrid molecules that consist of silica-oxygen cage functionalized with organic substituents [15]. POSS molecules exhibit a well-defined nanostructure and unique properties due to their hybrid structure that allows them to interact with polymeric matrix, and simultaneously introduce into the system inorganic silica cages [16]. The characteristic feature that makes POSS universal and interesting is the possibility of attaching various substituents (reactive and/or non-reactive) to the oxygen-silicon cage. The type of the substituent will determine not only the properties of the POSS itself, but also the interaction between the POSS and the polymer [17]. POSS bearing non-reactive substituents will form physical

✉ Konstantinos N. Raftopoulos
konstantinos.raftopoulos@pk.edu.pl

[1] Department of Chemistry and Technology of Polymers, Cracow University of Technology, ul. Warszawska 24, 31-155, Kraków, Poland

blend with polymeric matrix, while POSS possessing reactive substituents will covalently bond with polymer chain, and the nature of this bonding will depend on the functionality of the POSS (pendant, telechelic, bridge, bead, crosslink) [18]. Depending on the selected POSS type and the method of its introduction into the polymeric matrix, POSS moieties impact polymer properties in various ways [19]. By proper selection of the POSS type and of the introduction method, one may obtain composites with enhanced modulus, thermal stability, water tolerance, fire resistance, and dielectric properties, as well as reduced gas permeability, flammability, and heat release [4].

The introduction of POSS into hydrogel materials leads to enhanced mechanical properties [20–23], thermal stability [22], biocompatibility [23, 24], protein adsorption, and cell adhesion [25]. It may also lead to the induction of self-healing [21, 24] and shape memory properties [23]. The formulation of physical hydrogel/POSS blends or the introduction of POSS by ionic interactions is often associated with the problem of POSS agglomeration [26]. To overcome this issue, POSS is introduced into the matrix chemically (as a co-monomer in the polymerization process) [27].

POSS influence on NIPUs properties have been studied mainly in such systems. Chemical introduction of POSS into the matrix was carried out by using POSS that may react with amines, e.g. epoxy-functionalized POSS [28, 29], POSS bearing carbonate rings [30–33] or by using amino-functionalized POSS that reacts with cyclic carbonates [34, 35]. It was shown that bonding POSS into a polymer network may increase scratch resistance, thermal stability, and glass transition temperature, while simultaneously it decreases water absorption capacity. Despite numerous studies on the subject of NIPU/POSS composites, little attention has been devoted to the systems in which POSS is physically introduced into the polymer matrix.

Hence, our research covers study of NIPU/POSS composites obtained through physical introduction of octa(3-hydroxy-3-methylbutyldimethylsiloxy)POSS (8OHPOSS) into a PEO-based PHU network. Physical introduction of POSS bearing hydroxyl groups is not possible in conventional polyurethanes, at least in-situ during synthesis, however, in NIPUs such POSS should be physically restrained in the polymer matrix through hydrogen bonds, impacting the polymer in a new and different way than in conventional PUs. Studying NIPU/POSS physical blends where POSS is restrained by hydrogen bonds might be interesting from the point of view of molecule-polymer interactions that play important role, e.g. in drug delivery systems. In this study we show the influence of octa(3-hydroxy-3-methylbutyldimethylsiloxy)POSS (8OHPOSS) on the thermal stability, molecular mobility, and swelling of a PEO-based PHU network.

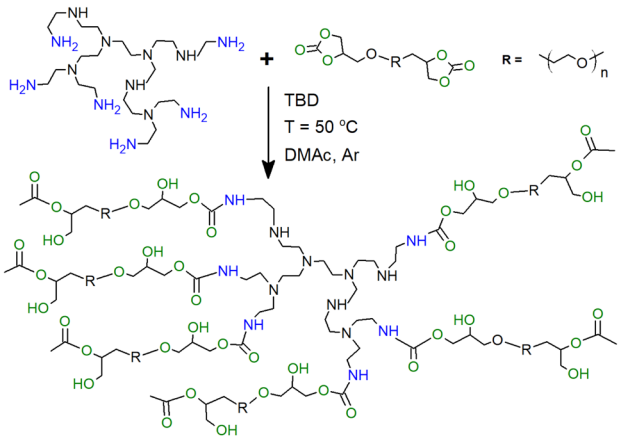

Scheme 1 NIPU network formation

Experimental

Materials

PEO-based bis(cyclic carbonate) (PEO-CC) of M_w~700 g/mol was purchased from Specific Polymers (Castries, France), polyethyleneimine (PEI) of M_w~600 g/mol, and 1,5,7-Triazabicyclodec-5-ene (TBD) were acquired from Sigma-Aldrich (Darmstadt, Germany). Octa(3-hydroxy-3-methylbutyldimethylsiloxy)POSS (8OHPOSS, POSS) was purchased from Hybrid Plastics (Hattiesburg, United States), and dimethylacetamide (DMAc) of 97% purity was obtained from Pol-Aura (Zabrze, Poland). All of the above materials were used as received. Phosphate buffer saline (PBS) concentrated solution was provided by Chempur (Piekary Śląskie, Poland), and diluted before use in accordance with the manufacturer's recommendations.

Synthesis

NIPU networks were synthesized in a one-step route (Scheme 1) by mixing all components in a three-necked flask equipped with a condenser, a gas supply system, and a sampling system. Cyclic carbonate and amine were added in the molar ratio of 1:1 carbonate rings to amino groups. The reaction was carried out at 50 °C under argon, using a magnetic stirrer. After reaction time of 150 min, upon significant increase of the viscosity, the mixture was transferred into a mold, so that gelation in the reactor could be avoided. Subsequently, the transferred mixture was conditioned in an oven at 90 °C to allow further crosslinking and DMAc evaporation.

Reaction progress was monitored by observing changes in FTIR spectra of the reaction mixture (Fig. 1). Formation

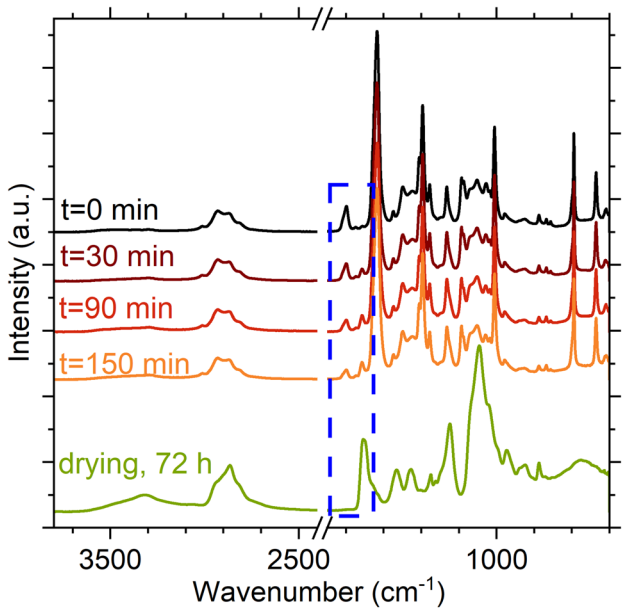

Fig. 1 FTIR spectra for monitoring reaction progress

of urethane moieties via opening of cyclic-carbonate rings was confirmed through formation of a band associated with the urethane-derived carbonyls (1710 cm^{-1}) at the expense of the carbonate-derived carbonyls (1800 cm^{-1}) [36]. After transferring reaction mixture into the drier and conditioning it for 72 h, no residual signals from cyclic-carbonyls were observed (complete disappearance of the band at 1800 cm^{-1}). 8OHPOSS (Fig. 2) was added at the beginning of the reaction, with all other raw materials, in amount of 1–10 wt% with respect to the polymer mass. Samples were labeled in terms of POSS content, with 0% standing for the pristine polymeric matrix.

Physico-chemical characterization

Fourier-transform infrared spectroscopy (FTIR)

Fourier-transform infrared spectroscopy (FTIR) was used to monitor reaction progress and to determine structure of the materials. Measurements were carried out using an ATR-equipped Thermo Scientific Nicolet iS5 spectrometer with a diamond crystal prism. Spectra were recorded in a wavenumber range of 4000 – 400 cm^{-1}, scanning resolution was 4 cm^{-1} with data gap 0.082 cm^{-1}.

Thermogravimetric analysis (TGA)

Thermogravimetric analysis was carried out to determine the thermal stability of the studied materials. Measurements were carried out under synthetic air, and nitrogen using a Netzsch TG 209 F1 Libra thermogravimetric analyzer with open crucibles (Al_2O_3). Measurements were carried out in the temperature range 30–600 °C (10 K/min) under inert atmosphere and 30–700 °C (10 K/min) in oxidative atmosphere.

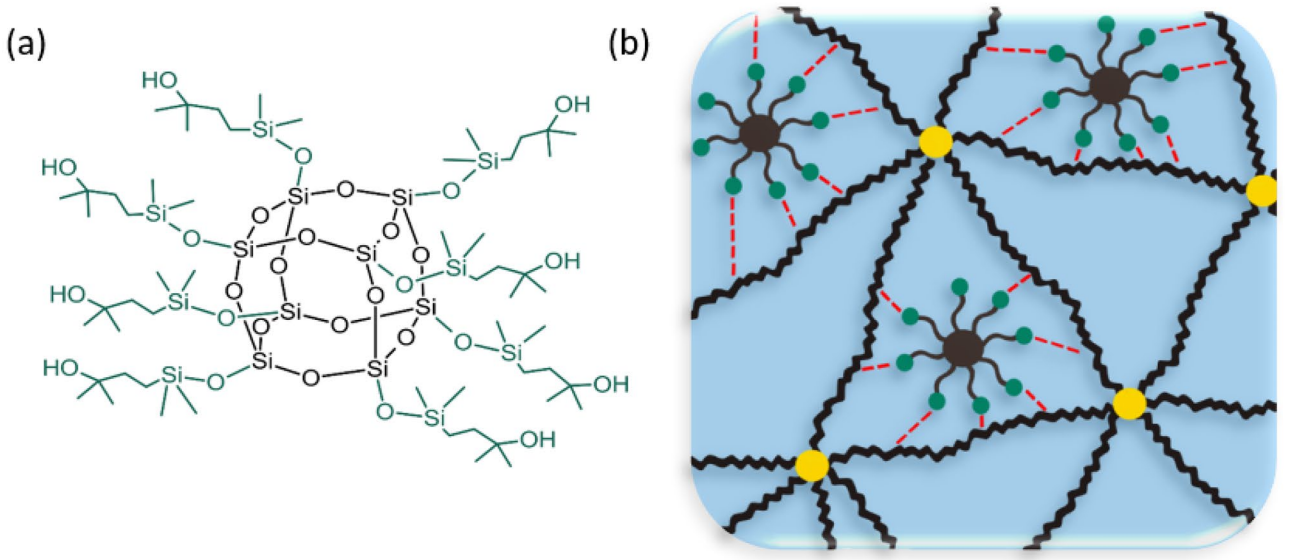

Fig. 2 **a** Structure of 8OHPOSS and **b** schematic spider-like representation of POSS incorporation into the matrix (green circles represent -OH groups in 8OHPOSS, red lines represent hydrogen bonds between POSS molecules and polymer chain, yellow circles represent crosslinking joints between PEG segments, black lines represent PEG segments)

Scanning electron microscopy (SEM)

Secondary electron images were recorded using a JEOL JSM-6010LA scanning electron microscope equipped with an EDS accessory. Prior to measurement, samples were coated with a gold layer of 4 nm nominal thickness. Images of the surface and cryo-fractured surfaces were taken. The working distance was set at 10 mm, and accelerating voltage was 10 kV.

X-ray diffraction (WAXD)

X-ray diffraction was applied to determine whether POSS form crystallites within the polymer matrices. Diffractograms were recorded using Bruker D2 PHASER diffractometer equipped with the LYNXEYE XE-T detector. Measurements were conducted in 2θ range of 6–60° with interval of 0.1° and acquisition time of 3 s.

Differential scanning calorimetry (DSC)

Differential scanning calorimetry was used to measure the glass transition temperature (T_g). Analysis was carried out using a Mettler Toledo 822e differential scanning calorimeter purged with argon and cooled with liquid nitrogen. Samples of 6–7 mg were measured in the temperature range − 100 to 30 °C (10 K/min); the reported T_g values were calculated as midpoint of the endothermic step. To eliminate the influence of water, prior to DSC measurements samples were dried over phosphorus pentoxide until their mass was equilibrated.

The glass transition temperature of highly crystalline 8OHPOSS was measured with an 823e Mettler Toledo calorimeter purged with Argon and cooled with an intracooler. Surprisingly this apparatus achieved faster cooling rates than the liquid nitrogen cooled one in the region of POSS crystallization. A heating scan was carried out from 25 to 180 °C (10 K/min) to melt the specimen, then the specimen was quenched as fast as the capacity of the apparatus allowed (rate set at 500 K/min, achieved > 50 K/min during crystallization) to -85 °C to avoid full crystallization. Subsequently, the specimen was heated up to 180 °C (10 K/min). The reported glass transition temperatures are midpoint values.

Dynamic mechanical analysis (DMA)

Dynamic Mechanical Analysis was carried out on a DMA 242 C Netzsch apparatus in tension mode in nitrogen environment with liquid nitrogen as a cooling medium. Heating rate was 2 K/min, frequency 5 Hz, and max. dynamic force 4 N. Specimens of approx. dimensions 0.5 × 5.0 × 7.0 mm were conditioned over phosphorus pentoxide before measurements, in order to remove any residual humidity.

Swelling/water uptake

Swelling/water uptake was measured by immersing dried polymeric samples (5 × 5 × 1 mm) in distilled water (DI) and phosphate-buffered saline (PBS) at temperature 37 °C. Mass of the conditioned samples $m_{hydrated}$ was measured after 30, 60, 120, 180, and 240 min, as well as after 24 h. Specimens were gently blotted with tissue paper before weighing to remove excess water from the surface. Water uptake *WU* was calculated by Eq. 1.

$$WU = \frac{m_{hydrated} - m_{dry}}{m_{dry}} 100\% \quad (1)$$

In which m_{dry} denotes the mass of the dry material before immersing it in water/PBS (data point taken as 0 min).

Characterization

Fourier-transform infrared spectroscopy

General structure

Figure 3 shows FTIR spectra of final materials. Bands at 3600 – 3100 cm^{-1} correspond to stretching vibrations of -OH and -NH- groups [37]. Bands at 3000 – 2750 cm^{-1} are associated with C-H stretching vibration in -CH_2- groups [38]. In the wavenumber range 1600–1750 cm^{-1} urethane-derived carbonyl bands of complex nature are observed [39]. The characteristic absorption peak at 1533 cm^{-1} correlates

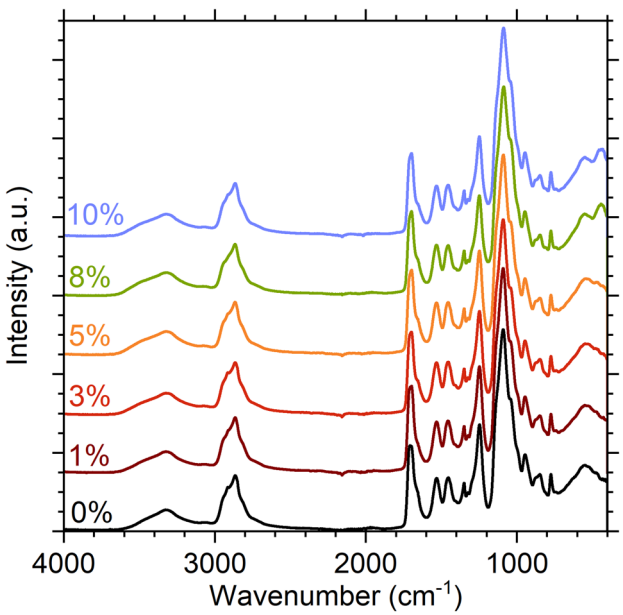

Fig. 3 FTIR spectra of synthesized NIPU networks

to bending of urethane-derived C-N-H and is typically observed in all polyurethanes [40, 41]. A strong band at $1180-950\ cm^{-1}$ corresponds to ether C-O-C (carbonate backbone) and alcohol C-O stretching vibrations [42].

Since POSS was introduced physically into the polymer matrix, it is expected that its influence on the materials morphology is associated with the impact of hydroxyl end-groups on inter- and intramolecular interactions, such as hydrogen-bonding. Thus, in order to quantify the influence of POSS on hydrogen bonding, the carbonyl region ($1800-1600\ cm^{-1}$) was studied in detail by fitting pseudo-Voigt functions in the form of Gaussian-Lorentzian sums (Eq. 2) (Fig. 4a).

$$y = 2A\left[\frac{s\sqrt{\ln 2}}{w\sqrt{\pi}}\exp\left(-4\ln 2\left(\frac{x-x_c}{w}\right)^2\right) + \frac{1-s}{\pi w\left[1+4\left(\frac{x-x_c}{w}\right)^2\right]}\right] \quad (2)$$

A - integral intensity, w - width of the band, x_c - the center of the band (location). s – shape parameter (shape parameter reflects the contribution of the Gaussian term to the sum: $s = 1$ means fully gaussian distribution, while $s = 0$ fully lorentzian one).

Carbonyl region

The carbonyl region of polyurethanes and poly(hydroxyurethanes) in general consists of three main components, that are usually associated with free carbonyls, hydrogen-bonded disordered carbonyls (carbonyls hydrogen-bonded in the soft phase), and hydrogen-bonded ordered carbonyls (carbonyls hydrogen bonded in hard domains) [37]. However, in case of non-segmented materials, such as the NIPUs at hand, the origin of the above-mentioned component needs to be sought elsewhere. The shift of band and their components is strongly influenced by hydrogen-bonds. It was shown that carbonyls forming more than one hydrogen bond exhibit stronger shift in comparison to carbonyls forming single hydrogen bonds [43]. Thus, the presence of three components in carbonyl region may be attributed to free carbonyls (carbonyls that do not form hydrogen-bonds, *free*), 'weakly' hydrogen-bonded carbonyls (carbonyls engaged in forming single hydrogen bond, *HB-1*) and 'strongly' hydrogen-bonded carbonyls (carbonyls that form double hydrogen bonds, *HB-2*).

Figure 4 shows results of performed fit - fitting curves (Fig. 4a) are shown for 5 wt% POSS composite as an example. Due to the large number of parameters to be determined, it was necessary to fix some of them in order to improve statistical significance of the rest. For this reason, a preliminary fit was performed in which we observed that the shape parameters s of the "free" peak was in the range 0.89–0.95 whereas s for the *HB-1* peak converged to 1 and for HB2 to 0. A second round of fitting was performed with s parameters fixed to 0.93, 1, and 0, respectively.

Upon POSS introduction, location x_c (Fig. 4b) of the *HB-2* component migrates to lower wavenumbers. Simultaneously, the location of the other components does not change significantly with POSS content, which means that the resultant difference in the position of the *free* and *HB-2*

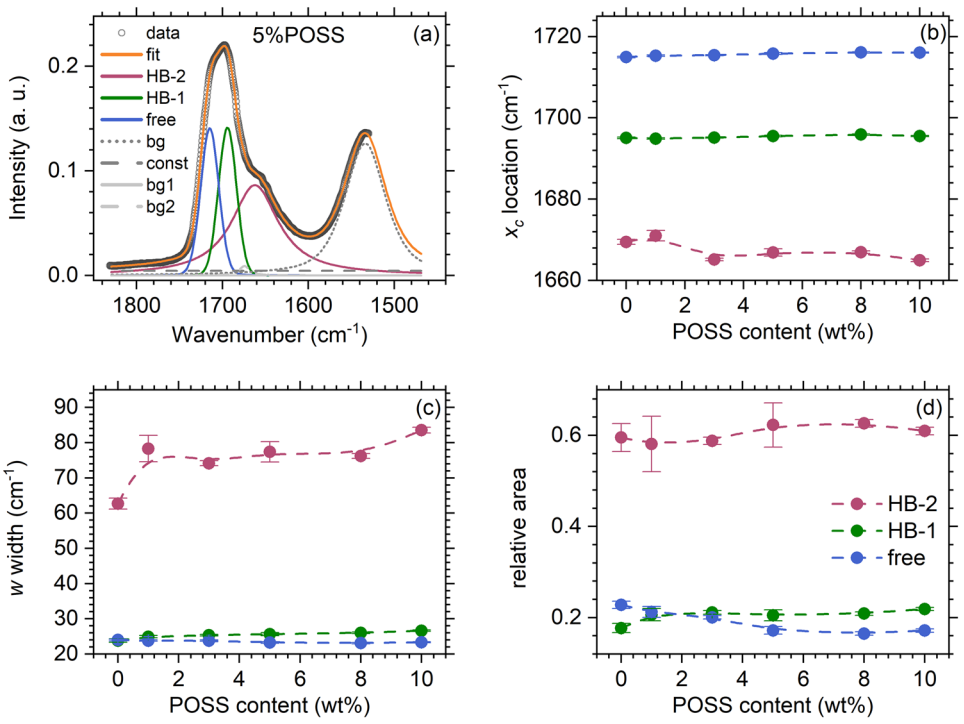

Fig. 4 Fitting of the carbonyl region: **a** fitting of the spectrum of a representative sample (5%), **b** location x_c of the peaks, **c** full width at half maximum w of the peaks, **d** area of the three carbonyl peaks normalized to the total area of the carbonyl components

components increases. The increase of the distance between the free component and components corresponding to hydrogen-bonded moieties indicates an increase in the strength of the hydrogen-bonding [44]. Increase in the shift of *HB-2* component with increasing POSS content may originate from the fact that introducing -OH end-capped 8OHPOSS into polymer matrix results in formation of hydrogen bond between carbonyls and -OH groups instead of -NH- moieties (-C = O ··· HO- hydrogen bonds being stronger than -C = O ··· HN- ones) [45].

The width of the component depends mainly on the enthalpic landscape of the studied moiety, namely the polydispersity of strengths of intermolecular interactions (e.g. hydrogen-bonding) [46]. Here, upon increasing POSS content, broadening of the *HB-2* component is observed (Fig. 4c). The broadening may result from higher dispersity of hydrogen bonds strength, which is in accordance with observed changes in components location upon POSS introduction. The width of *HB-1* component increases, but to a negligibly small extent, while the width of free band remains stable as expected.

With increasing POSS content, contribution of *HB-1* and *HB-2* components to the total intensity of the carbonyl band (Fig. 4d) increases at the expense of *free* component, showing that 8OHPOSS introduction allows for formation of new hydrogen bonds between carbonyls and POSS-derived OH groups.

POSS dispersion

XRD diffractograms of 8OHPOSS and studied NIPUs are shown in Fig. 5. Interestingly, there are no traces of crystalline peaks on the diffractograms of the composites despite the highly crystalline nature of 8OHPOSS. Uniform POSS dispersion is maintained even at high POSS loading, exhibiting dispersion comparable [47] or even better [48, 49] than in systems where POSS is covalently incorporated into a polyurethane network. Uniform POSS dispersion in physically modified composites results from compatibility between the polar matrix and the polar -OH groups at the end of 8OHPOSS substituent groups. POSS-derived hydroxyl groups may form hydrogen bonds with moieties in the matrix, such as (i) carbonyls, (ii) hydroxyls, (iii) secondary amines, and (iv) ethers, which allows for uniform POSS dispersion even at high 8OHPOSS concentrations.

To confirm good POSS dispersion, SEM-EDS analysis was performed for the composite with the highest POSS loading (10 wt%). Images of the surface and fracture are shown in Fig. 6. Scarce POSS agglomerates were observed on the surface of the material, while in the bulk POSS distribution remained homogenous. Uniform POSS dispersion in the composite with the highest content of filler allowed to assume a good dispersion in composites with lower POSS loading.

This shows that proper selection of POSS type allows for utilizing intermolecular forces to restrain POSS crystallization and obtaining uniform dispersion observed commonly for systems in which POSS moieties are chemically bonded to the polymer [50].

Thermal stability

Figures 7 and 8 show TG and DTG curves recorded in inert and oxidative atmosphere, respectively. The chain stability and the efficiency of POSS molecules as heat stabilizers were tested under inert atmosphere to eliminate effects from autooxidation and secondary reactions, and in air to test thermal stability in the processing/application conditions [51].

The studied materials exhibit a two-step degradation in inert atmosphere and a three-step decomposition path in oxidative atmosphere, as is usually observed for conventional polyurethanes [52–54] as well as for some NIPUs [55, 56].

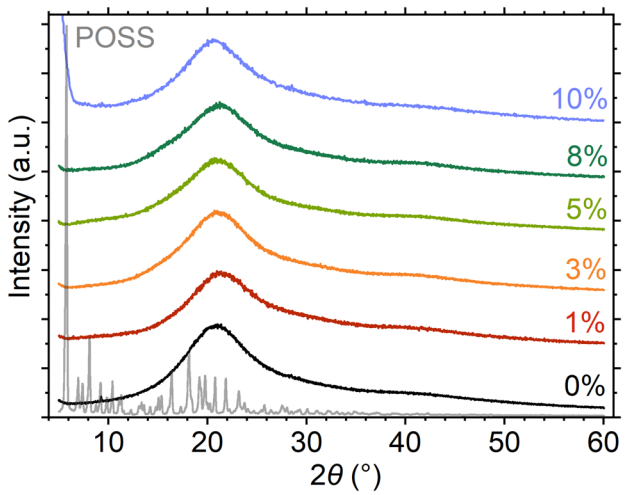

Fig. 5 WAXD diffractograms of 8OHPOSS and studied NIPUs (translated)

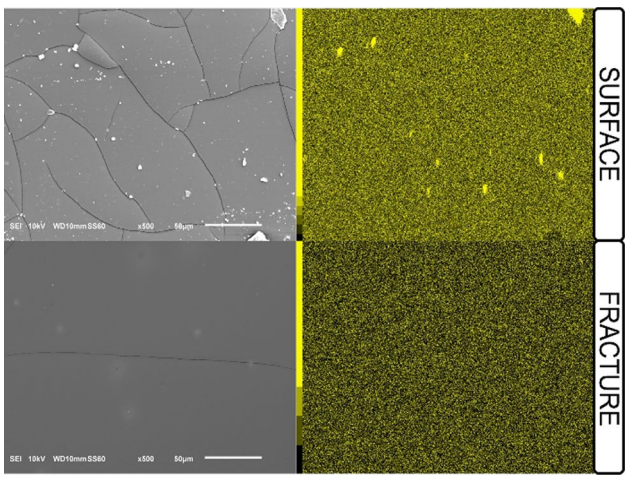

Fig. 6 SEM microphotographs x500 with Si mapping

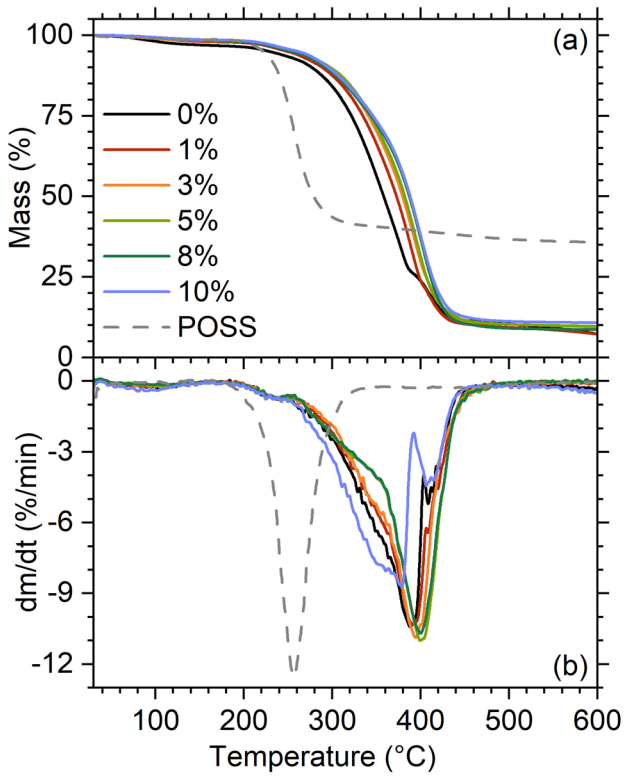

Fig. 7 **a** TG and **b** DTG curves recorded under nitrogen

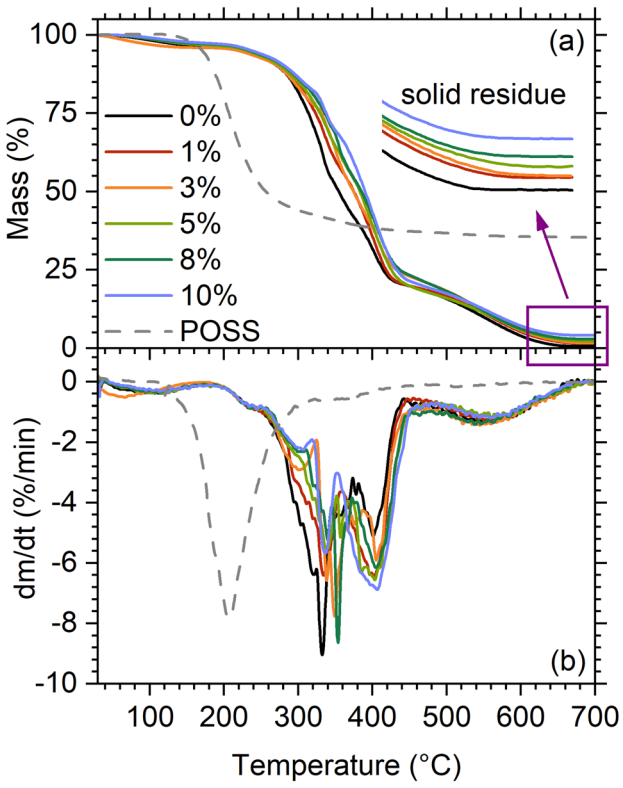

Fig. 8 **a** TG and **b** DTG curves recorded under synthetic air

The first degradation step is associated with the scission of the most thermally labile moieties, i.e. urethane groups [54, 56, 57]. The second step of NIPUs degradation is attributed to the scission of ether linkages [58, 59], which here are present in the backbone of PEO-based carbonate. The additional degradation step in oxidative atmosphere originates from further oxidation of residual degradation products at higher temperatures [60]. For the studied materials, the first and the second degradation steps in inert environment strongly overlap, and are present in the temperature range 255–450 °C, while in oxidative one they are more distinguishable with the first step occurring at 265–350 °C, and the second one at 350–450 °C. The materials studied in the course of this work exhibit degradation temperature range similar to other NIPU thermosets reported in the literature [55]. Mass of the solid residue in oxidative atmosphere (Fig. 8) increases with increasing POSS content, as expected.

With increasing POSS content, the onset of the degradation temperature increases in both inert and oxidative atmospheres (Fig. 9), even though the POSS itself exhibits lower degradation temperature onset than pristine matrix. The above shows that 8OHPOSS is suitable to be used as a thermal stabilizing agent for nonisocyanate polyurethanes. The stabilizing effect is particularly pronounced in inert atmosphere.

Improving thermal stability of polyurethanes upon POSS introduction is not always the case [47, 61–63], since proper selection of POSS type in regard to polymeric matrix is crucial (e.g. to avoid formation of thermally labile ureas). Enhancement of thermal stability in PU/POSS composites was reported before, but mainly for composites in which POSS was covalently incorporated into a polymeric chain [64, 65]. This study shows that selecting a proper type of POSS allows for increased thermal stability in NIPUs even upon physical introduction of POSS into polymeric matrix.

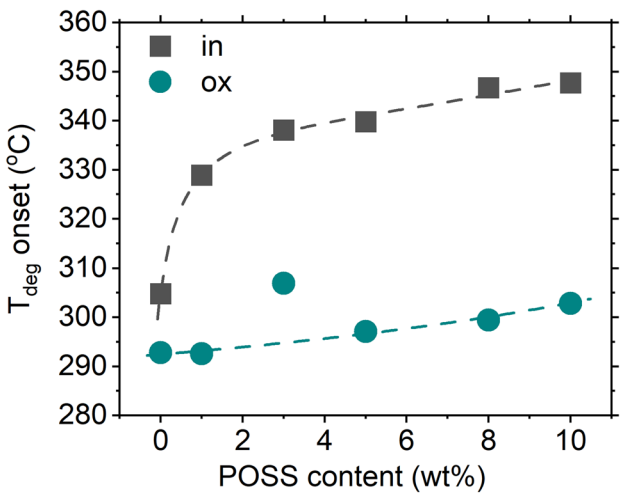

Fig. 9 Degradation temperature onset as a function of POSS content

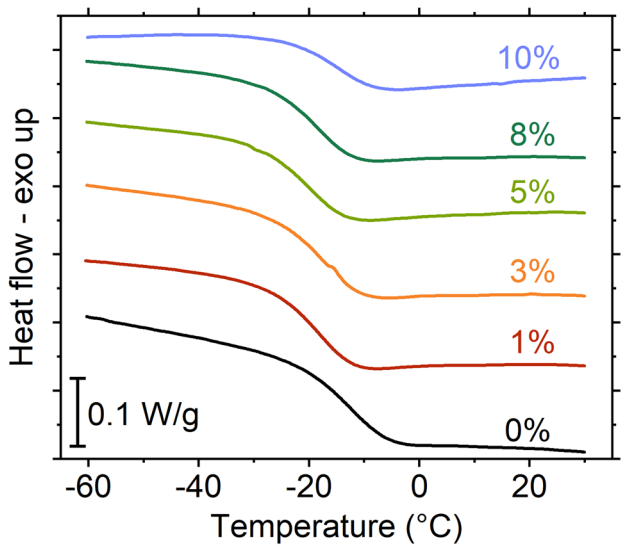

Fig. 10 DSC curves (translated) of studied NIPUs

Thermal stability increase even at high POSS loadings also indicates good POSS dispersion, since forming POSS agglomerates in POSS/polymer composites was reported to cause no change or even result in decrease in thermal stability upon increasing POSS loading [51]. The above stays in agreement with results obtained from XRD and SEM-EDS analyses.

Increasing thermal stability of the material by POSS incorporation is usually associated with formation of a rigid silicate-based barrier that decreases evaporation of volatiles and restricts gaseous fuel access to the bulk [64]. Interestingly, the step observed for POSS on TG and DTG curves does not occur in the composites, which may suggest that good POSS dispersion allows for the polymer matrix to shield thermally labile POSS substituents. Therefore, it may be argued that POSS substituents degradation occurs simultaneously with scission of urethane moieties, however, the formed silica residue protects polymer matrix and delays further thermal decomposition.

Molecular mobility

The calorimetric glass transition was studied by DSC. Figure 10 shows raw DSC curves of the dried materials in the glass transition region. POSS introduction into NIPU network causes a decrease in glass transition temperature (T_g) (Fig. 11), i.e. plasticization. Since 8OHPOSS was introduced physically into the polymeric matrix, it acts as a so-called external plasticizer, interacting with the polymer without chemical reaction [66]. Plasticizing effect of POSS is a well-known phenomenon and is usually explained by synergic effects of the free volume increase, chain friction reduction, and decrease in entanglement density [67].

Although all composites exhibit T_g lower than the matrix, increasing POSS content over 5 wt% causes a slightly increasing trend in T_g. This phenomenon might result from two factors: (1) the effect of increased density of hydrogen-bonded carbonyls at the expense of free ones (as shown by FTIR fitting results) takes over and dominate the effect of free volume increase; (2) at high POSS loadings (8 wt% and 10 wt%) rigid silica cages concentration reaches its critical point and those rigid structures begin to slightly hinder molecular mobility of the polymer. The detailed discussion and explanation is given below.

Taking into account the polymer structure, mainly presence of -OH, -NH- and C = O groups, one expects rather strong interactions between POSS and the matrix due to

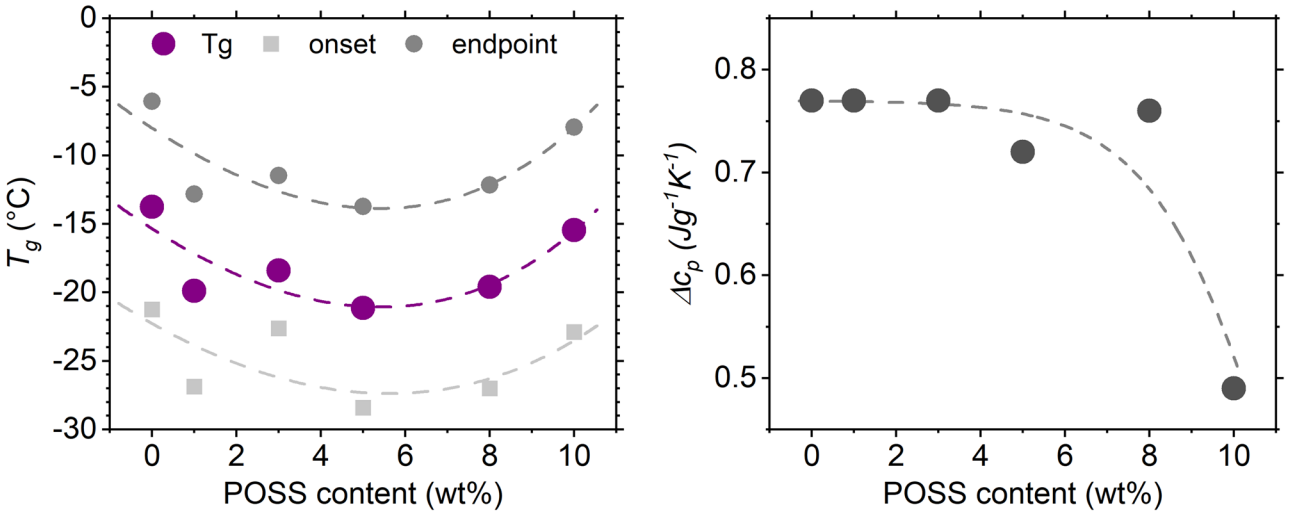

Fig. 11 **a** Calorimetric glass transition temperature as a function of POSS content: onset, endpoint and midpoint, **b** Δc_p of a glass transition as a function of POSS content

formation of hydrogen bonds, which is supported by the results of the FTIR carbonyl region fitting (Fig. 4). Thus, the decrease of T_g upon POSS introduction (Fig. 12) into the matrix seems counterintuitive, especially since attractive interaction between polymer chain and POSS particles would result in "binding" polymer chain on the relatively rigid structure of POSS cage and restricting polymer mobility (increasing T_g) [18].

It was explicitly shown by Young et al. [68] that physical introduction into polymeric matrix of octa functional POSS (without measurable T_g), end-capped with groups able to form hydrogen bonds with polymer chains, results in increase of glass transition temperature due to increase in hydrogen bonding (increase in attractive forces that slow down mobility). Introducing POSS with measurable T_g below that of the polymer, functionalized with groups that may form hydrogen bonds with polymer, lowered composites T_g. The reason is that now the composites consist of two components, with different glass transitions and they follow mixing laws [69, 70] giving intermediate T_g values. Noteworthy, this phenomenon has been observed also in other polymer-POSS systems [18, 68, 71, 72].

On the other hand, the observed plasticization means that 8OHPOSS-8OHPOSS, polymer-polymer, and polymer-8OHPOSS intermolecular forces are of the same order of magnitude [66]. This is supported by the fact that with an increasing POSS content no broadening or narrowing of glass transition is observed, meaning there is no significant change in dynamic heterogeneity in the composites compared to the pristine matrix [68]. The occurrence of equally strong interactions between the polymer chain and POSS molecules shows strong influence of hydroxyl groups at the ends of the silicon cage substituents on the POSS interaction with the matrix. Thus, it may be concluded that POSS-derived hydroxyl groups dominate POSS properties, enable 8OHPOSS molecules to strongly interact with the polymeric matrix, and subsequently allow POSS to infiltrate between polymer chains, disturb attractive forces between polymer molecules, increase free volume of the material, and promote decrease in T_g (plasticization).

To investigate the discussed possibilities, T_g of 8OHPOSS was measured as described in 2.2.5. The weak step observed on heating curve at temperatures below the temperatures of cold crystallization is a glass transition of amorphous POSS phase. The step is accompanied by a small peak associated with enthalpy relaxation [73].

Interestingly, T_g of 8OHPOSS was observed around 3 °C, which is significantly higher than the T_g of pristine matrix (-14 °C), showing that mixing laws, such as that of Fox [69], do not apply here. This is due to the fact that POSS may influence glass transition by many different mechanisms, and usually the observed effect is the result of different 'overlapping' mechanisms [18]. Moreover, the resultant change of given mechanism might be different, based on the properties of the POSS itself. Except from mentioned "mixing" of dynamics and hindering of chain-chain attractive interactions, POSS may also act as a nanoparticle. In regard to polymers' T_g, nanoparticles are considered relatively large immobile structures that may promote formation of rigid amorphous fraction (RAF), and thus constrain mobility by confinement [74]. Effect of RAF formation gives no distinct thermal response, however it might be observed as a deficit in Δc_P [75]. The deficit in Δc_P is clearly observed for 10 wt% composite, indicating that 'nanoparticle' mechanism might play an important role in POSS impact on polymer mobility at high POSS concentrations.

Here, we would like to propose an explanation for observed changes in mobility upon POSS introduction in the studied systems. It is noteworthy that for NIPUs at hand the most hydrophilic/polar chain segments are located just beside junction points. At low concentration, POSS molecules most probably penetrate between the polymer chains and locate themselves at the centers of polarity, i.e. close to PEI chains, thus effectively immobilizing them. This immobilization of PEI segments increases mobility of PEG chains between junctions. Moreover, the above does not rule out that the penetration of POSS molecules between the polymer chains could not increase the distance between the chains (increase in free volume). Both of aforementioned behaviors would act in favor of decreasing T_g, as is observed up to 5 wt% of POSS loading. Further increasing of POSS content would force molecules to locate e.g. between PEG segments, possibly forming bridges that slightly decrease mobility. Finally, at 10 wt% the RAF is created and the systems mobility decreases further.

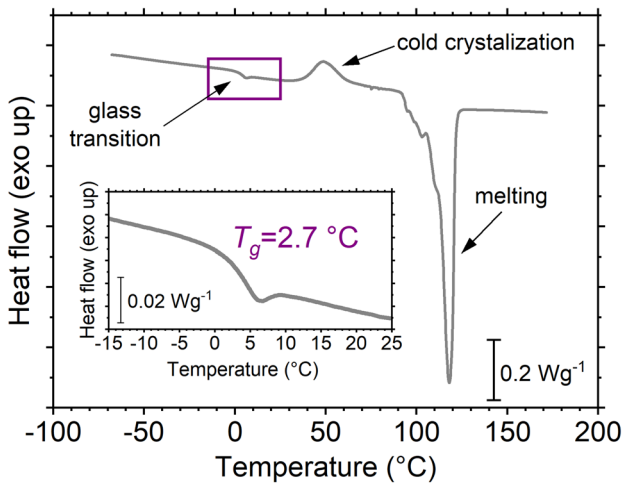

Fig. 12 DSC heating curve for 8OHPOSS after rapid cooling

Termomechanical properties

The values of storage modulus in glassy region (E'_{glass}) of the NIPUs at hand (Fig. 13a) are in the range of 1000–3400 MPa (at − 40 °C). With increasing temperature, storage modulus (E') decreases and forms a step associated with the dynamic glass transition (α relaxation). After this step, the rubbery plateau is observed up to high temperatures (90 °C), which is typical for thermoset polymers [76].

POSS influence on mechanical properties of studied NIPUs is non-monotonic. In general, POSS loading seems to slightly lower the modulus (E') in comparison to pristine matrix. The lowest modulus is observed for 8 wt% POSS loading. An increase in the mechanical performance is observed of composites containing 5 wt% and 10 wt% of POSS, with 5 wt% composite having the highest modulus out of all studied materials. Introducing POSS in lower amounts (1–8 wt%) allows for enhancing materials' mechanical stability at higher temperatures (30–80 °C). The enhancement of polymer mechanical properties by POSS for composites where the POSS in chemically built into the matrix is usually correlated with incorporation of network junction points with increased toughness. For physical blends, such as the studied hybrid composites, it should be sought in the presence of interactions resulting from hydrogen bonds between polymer and POSS that leads to interfacial adhesion [77]. However, 10 wt% POSS content contributes to the brittleness of the material, which is observed as specimen breakage at lower temperatures in comparison to pristine matrix (Fig. 13a). The increased brittleness of 10 wt% composite might result from increased macrochain tension in the network filled with bulky silsesquioxane cages.

The step in $E\prime$ is accompanied by a sharp peak in tanδ curves (Fig. 13b). The maximum temperature of tanδ (T_α) is a good measure of the glass transition temperature [78]. Figure 14 shows the comparison between T_α and the calorimetric T_g.

It is well-known that the values of glass transition temperatures determined by different methods give different values due to different heating rates and frequencies of measurements [79, 80]. However, usually the correlation in temperature trends is observed [6, 74]. Here, however, the trend observed for calorimetric glass transition (T_g) is not the same as for dynamic one (T_α). While the DSC suggests plasticization in the whole range of POSS content, lowering of T_α in comparison to pristine matrix is only observed for composites with 3 wt% and 8 wt% POSS loading. Such a discrepancy between methods has been observed in the past in such complex systems [81], and has been attributed to the complexity of the alpha relaxation: it is possible that modes of different mobility, contributing to the glass transition, have different sensitivity to different stimuli.

Crosslinking density

The crosslinking density of studied hybrid materials was calculated based on rubbery modulus as proposed by Zhao and Abu-Omar [82] (ρ_{DMA}, Eq. 3) and based on a chemistry of composition as proposed by Hill [83] (ρ_{comp}, Eq. 4) with assumption of ideal network formation and the influence of

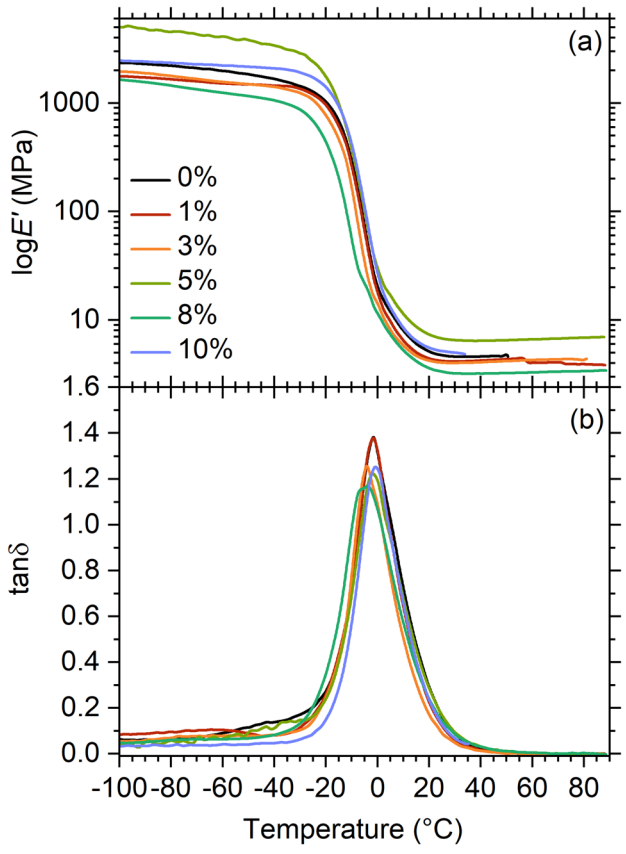

Fig. 13 DMA curves recorded for studied NIPUs at 5 Hz: **a** storage modulus and **b** loss tangent as a function of temperature

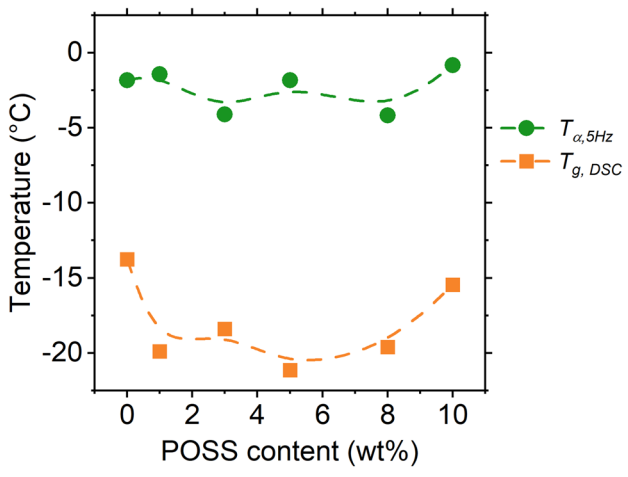

Fig. 14 Comparison of calorimetric and dynamic glass transition temperatures as a function of POSS content

mass fraction of POSS. The assumption of ideal network formation is based on FTIR showing full conversion of cyclic-carbonate ("Fourier-transform infrared spectroscopy"). The calculated values of crosslink densities are given in Table 1.

$$\rho_{DMA} = \frac{E'_T}{RT} \tag{3}$$

E'_T is rubbery modulus at 22 °C, $R$is gas constant, and T is absolute temperature at which the modulus values were taken.

$$\rho_{comp} = \frac{nd_{material}}{(M_{network} + cM_{network})} \tag{4}$$

c is POSS mass fraction (for matrix $c = 0$, for the composite with 10 wt% POSS $c = 0.10$), $d_{material}$ – the density of the material, n is moles of crosslinks per network unit and $M_{network}$ is molar mass of the network unit, as defined by [83].

The values calculated based on the chemistry of composition give crosslinking density of the same order of magnitude as the crosslinking density determined on the basis of rubbery modulus. The differences between the values obtained through different approaches might result from the additional effects that influence the modulus, which are not taken into consideration in calculations based on composition. Nevertheless, the fact that presented values are in the same order of magnitude shows that for studied materials the assumption of ideal network is a good approximation of the real network morphology.

Table 1 Crosslink densities calculated on the basis of rubbery modulus (ρ_{DMA}) and chemistry of composition (ρ_{comp})

Material	ρ_{DMA}	ρ_{comp}
0%	1.94	2.35
1%	1.71	2.28
3%	1.65	2.68
5%	2.78	2.51
8%	1.37	1.95
10%	2.14	2.18

Swelling

Swelling of studied NIPUs was measured in distilled water and in phosphate buffer saline (PBS, pH = 7.4) at 37 °C. The studied NIPUs exhibit high absorption capacity up to 200 wt% in distilled water, and 215 wt% in PBS. The absorption process consists of two stages (Fig. 15): the first (0-240 min) is connected with a rapid increase in the amount of absorbed water; and the second one is the stage of slow absorption and/or equilibration [7, 84, 85].

Interestingly, for both media, the hydrogel with the highest POSS content (10 wt%) showed the highest uptake, while the general influence of POSS introduction into the matrix was inverse for materials immersed in water and PBS. Composites up to 8 wt% POSS absorbed less in water in comparison to pristine matrix, which is most probably the result of the presence of the hydrophobic silica cages [86]. However, POSS-loaded composites exhibit higher water uptake than the matrix, when immersed in PBS, showing that physically incorporated 8OHPOSS promotes water uptake in saline solutions. The above shows dependence opposite to that, which is usually reported in the literature, i.e. that POSS addition tends to lower swelling ratio/water uptake when incorporated chemically into the matrix [86, 87].

Water uptake rate shows similar behavior in PBS and distilled water (DI) at the initial absorption stage (0–60 min). At later stages, differences in specimens behavior depending on the conditioning medium are beginning to become apparent. NIPUs submerged in DI show stabilization after 3 h, while specimens immersed in PBS exhibit further slow absorption.

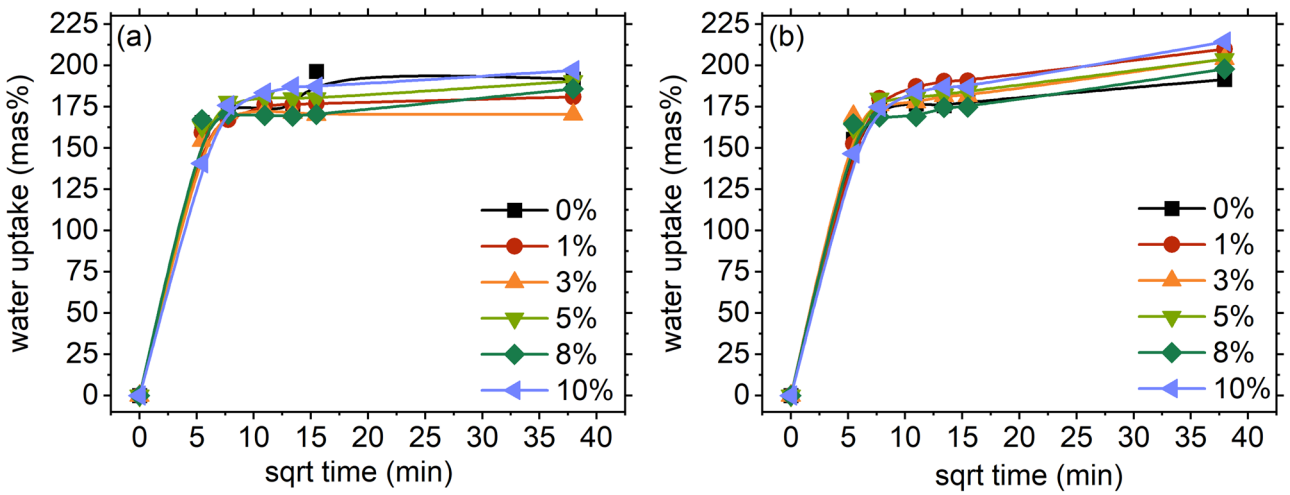

Fig. 15 Water uptake rate of studied specimens in **a** distilled water and **b** PBS

Despite different swelling behavior, water uptake after 24 h for NIPU matrix was the same in both media, while hydrogels modified with POSS exhibit higher medium absorption (swelling) in PBS (containing Na^+, K^+, PO_4^{2-}, HPO_4^- and Cl^- ions) than in DI. The above is in contradiction to what is usually reported for other hydrogel materials, i.e. swelling/absorption capacity decreases with increasing salinity of a medium [88–90]. Decreasing absorption with increasing salinity of the medium is usually connected with charge shielding effect of ions that reduces swelling [12, 91] or in case of PEG-based hydrogels lower swelling in PBS than in DI might originate from partial salting out of the PEG components in the ionic PBS solution [92]. Here, the hydrogel matrix does not show the absorption decrease upon increasing salinity, which may result from the presence of multiple –CONH– bonds, that are able to mitigate the charge shielding effect of ions [12], and from high crosslink density which prevent salting out of PEG components. Since for the pristine matrix there is no dissimilarity in swelling in different media, the increase of composites hydrogels' water uptake in PBS in comparison to DI must then result from the presence of POSS. Increasing swelling with increasing POSS content is usually discussed in POSS-crosslinked hydrogels, and attributed to decreasing cross-link density of the hydrogels [92]. Since this is not the case for hydrogels under consideration, one should take into account other factors determining the above phenomenon. It is possible that 8OHPOSS promotes swelling in PBS due to interactions between the POSS and ions in the solution. To confirm this hypotheses, however, further studies are required.

To determine differences in composites swelling between media, two types of calculation were conducted: (1) relative water uptake difference in both media at 24 h was calculated as given in Eq. 5 (approach 1); (2) for data points obtained in the time scale 0-240 min, Voigt model (Eq. 6) was fitted as proposed by Zhang et al. [85] (Fig. 16a), and, subsequently, differences of quantified swelling at equilibrium (S) between media was calculated analogously as for the data at time point of 24 h (approach 2). The second approach was conducted due to lack of evident equilibrium at swelling curves for hydrogels conditioned in PBS – water uptake for the specimen was increasing up to 300 wt% after 70 h of conditioning and after that time the further water uptake could not be measured due to specimen fragmentation.

$$\Delta swell = \frac{WU_{PBS} - WU_{H2O}}{WU_{H2O}} 100\% \tag{5}$$

$\Delta swell$ – swelling difference (difference of hydrogels swelling in PBS and distilled water in relation to swelling in distilled water), $WU_{PBS,24h}$ - water uptake after 24 h in PBS, $WU_{H2O,24h}$ - water uptake after 24 h in DI

$$S_t = S\left(1 - \exp\left(\frac{-t}{r}\right)\right) \tag{6}$$

S_t – water uptake at a given time point, S – water uptake at equilibrium (at inifite time), t – time in minutes, r– time required to reach 0.63 of the equilibrium water uptake.

Both approaches give similar trends of POSS influence on promoting swelling in saline solution (Fig. 16b). The most pronounced differences are observed at low POSS

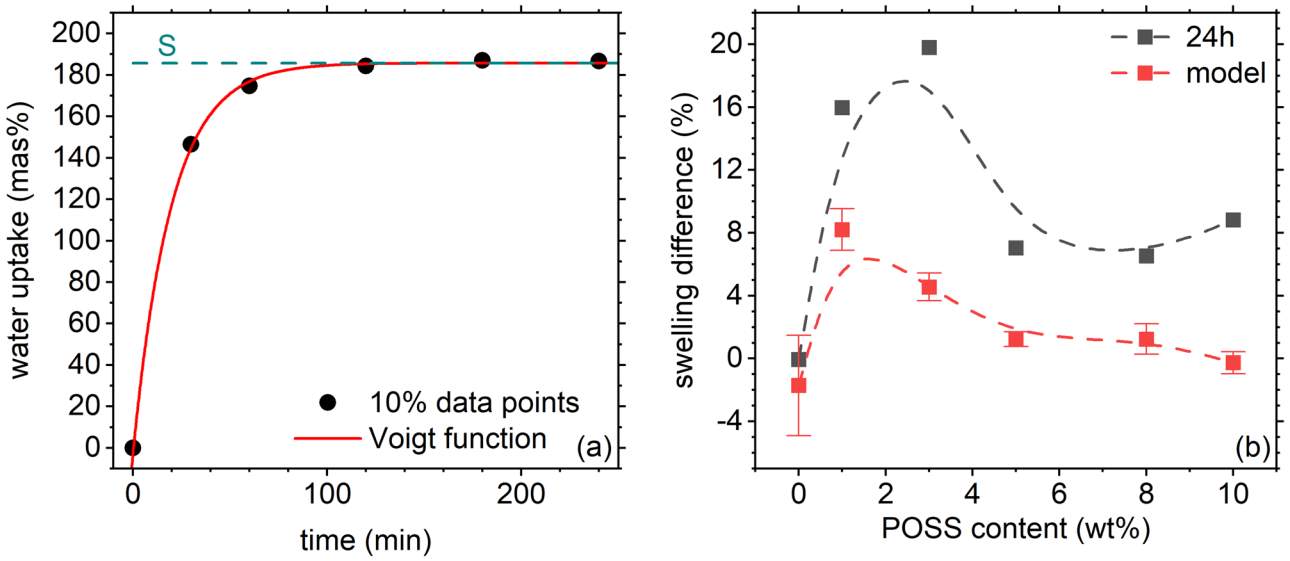

Fig. 16 **a** Model fitting to the data of representative specimen (10 wt% composite), **b** difference of swelling after 24h (grey) and in the 'infinite' time (red) as a function of POSS

loadings (1–3 wt%), while at higher POSS concentration this difference declines. The disparity between presented data calculated based on a water uptake at 24 h and on the model lay mostly in numbers, showing that proposed model can be used to determine trends, however, it may not necessarily be quantitative. The difference between taken approaches may also result from strong effect of third absorption stage and long-time equilibration. The increase of hydrogel swelling in PBS compared to DI is up to 20% (for 3 wt% composite) for data at 24 h and up to 8% (for 1 wt% composite) for the data predicted by the applied model.

Conclusions

POSS-modified PEO-based non-isocyanate polyurethane networks that are capable of acting as hydrogels have been successfully synthesized. The selection of POSS with polar OH groups at the ends of the alkyl substituents allowed uniform dispersion of POSS in the polar polymer matrix, even at high POSS loadings. Uniformly dispersed 8OHPOSS, despite bearing oxygen-rich hydroxyl groups, acts as a thermal stabilizer of NIPU matrix, increasing degradation temperature onsets in both oxidative and inert atmospheres.

Introducing POSS into the matrix slightly modifies molecular mobility. 8OHPOSS reduces calorimetric (T_g) in the whole studied POSS loading range (1–10 wt%), however, at higher POSS contents the dropping trend in T_g gets reversed and a slight increase is observed, which shows that the mechanism of POSS impact on glass transition changes at high POSS loadings. At low concentrations POSS molecules penetrate into hydrophilic centers around junction points, immobilizing them and simultaneously increasing mobility of PPO chains, while at high concentrations POSS molecules may form RAF structures or create bridges between macrochains, slightly increasing the calorimetric glass transition temperature. Dynamic glass transition (T_α) seems to be unaffected by POSS introduction.

NIPU matrix exhibits similar swelling in distilled water and PBS. 8OHPOSS impacts swelling differently, depending on the medium – it reduces distilled water uptake while promotes swelling in PBS, which is contradictory to usually reported behavior of hydrogels. Thus, 8OHPOSS may act as a swelling enhancer in PBS solution. Comparison of the crosslinking density values obtained through calculation based on chemical composition and rubbery modulus show values of the same order of magnitude, indicating that mechanical behavior of studied networks is very similar to that of ideal network.

The studied materials are interesting from the point of view of biomedical applications, such as hydrogel wound dressings or polymer drug delivery systems. Therefore, studying such composites in regard to hydration mechanisms, biocompatibility, and drug release kinetics could be next steps for obtaining environment-friendly, safe and multi-purpose biomedical materials. Such studies are now in progress.

Acknowledgements This research was funded by the National Research Center in Poland (Narodowe Centrum Nauki, NCN), under contract number 2017/27/B/ST8/01584. We thank Paulina Zając, MSc (CUT) for performing thermogravimetric analysis experiments and assisting with their analysis. All fitting procedures were carried out with software *Grafity*, created and freely distributed (grafitylabs.com) by Dr. Daniel Fragiadakis, to whom we express our gratitude.

Declarations

Conflict of interests The authors declare no competing financial or non-financial interests that are directly or indirectly related to this work.

References

1. Gomez-Lopez A, Elizalde F, Calvo I, Sardon H (2021) Trends in non-isocyanate polyurethane (NIPU) development. Chem Commun 57:12254–12265. https://doi.org/10.1039/D1CC05009E
2. Rokicki G, Parzuchowski PG, Mazurek M (2015) Non-isocyanate polyurethanes: synthesis, properties, and applications. Polym Adv Technol 26:707–761. https://doi.org/10.1002/pat.3522
3. Kathalewar MS, Joshi PB, Sabnis AS, Malshe VC (2013) Non-isocyanate polyurethanes: from chemistry to applications. RSC Adv 3:4110–4129. https://doi.org/10.1039/c2ra21938g
4. De Rossi KMF, Alves VS, Noeske PLM et al (2019) Hybrid films based on nonisocyanate polyurethanes with antimicrobial activity. In: Grumezescu A, Holban AM (eds) Materials for Biomedical Engineering: bioactive materials for Antimicrobial, Anticancer, and Gene Therapy, 1st edn. Elsevier, pp 77–116
5. Guan J, Song Y, Lin Y et al (2011) Progress in study of non-isocyanate polyurethane. Ind Eng Chem Res 50:6517–6527
6. Raftopoulos KN, Łukaszewska I, Bujalance Calduch C et al (2022) Hydration and glass transition of hybrid non-isocyanate polyurethanes with POSS inclusions. Polymer 253:125010. https://doi.org/10.1016/j.polymer.2022.125010
7. Gennen S, Grignard B, Thomassin JM et al (2016) Polyhydroxyurethane hydrogels: synthesis and characterizations. Eur Polym J 84:849–862. https://doi.org/10.1016/J.EURPOLYMJ.2016.07.013
8. Khatoon H, Iqbal S, Irfan M et al (2021) A review on the production, properties and applications of non-isocyanate polyurethane: a greener perspective. Prog Org Coatings 154:106124. https://doi.org/10.1016/J.PORGCOAT.2020.106124

9. Błażek K, Datta J (2019) Renewable natural resources as green alternative substrates to obtain bio-based non-isocyanate polyurethanes-review. Crit Rev Environ Sci Technol 49:173–211. https://doi.org/10.1080/10643389.2018.1537741
10. Bourguignon M, Thomassin JM, Grignard B et al (2019) Fast and facile one-pot one-step preparation of nonisocyanate polyurethane hydrogels in water at room temperature. ACS Sustain Chem Eng 7:12601–12610. https://doi.org/10.1021/acssuschemeng.9b02624
11. Fanjul-Mosteirín N, Aguirresarobe R, Sadaba N et al (2021) Crystallization-Induced Gelling as a method to 4D print low-water-content non-isocyanate polyurethane hydrogels. Chem Mater 33:7194–7202. https://doi.org/10.1021/ACS.CHEMMATER.1C00913
12. Wang Y, He G, Li Z et al (2018) Novel Biological Hydrogel: Swelling Behaviors Study in Salt Solutions with Different Ionic Valence Number. Polymers (Basel) 10. https://doi.org/10.3390/POLYM10020112
13. Bourguignon M, Thomassin J, Grignard B et al (2021) Water-Borne Isocyanate-Free polyurethane hydrogels with adaptable functionality and behavior. Macromol Rapid Commun 42:2000482. https://doi.org/10.1002/marc.202000482
14. Bae SW, Kim J, Kwon S (2022) Recent advances in Polymer Additive Engineering for Diagnostic and Therapeutic Hydrogels. Int J Mol Sci 23:2955. https://doi.org/10.3390/IJMS23062955
15. Chen F, Lin F, Zhang Q et al (2019) Polyhedral Oligomeric Silsesquioxane Hybrid polymers: well-defined Architectural Design and potential functional applications. Macromol Rapid Commun 40:1900101. https://doi.org/10.1002/MARC.201900101
16. Shi H, Yang J, You M et al (2020) Polyhedral Oligomeric silsesquioxanes (POSS)-Based hybrid soft gels: Molecular Design, Material advantages, and emerging applications. ACS Mater Lett 2:296–316. https://doi.org/10.1021/acsmaterialslett.9b00491
17. Kannan A, Muthuraj C, Mayavan A, Gandhi S (2023) Multifaceted applications of polyhedral oligomeric silsesquioxane and their composites. Mater Today Chem 30:101568. https://doi.org/10.1016/J.MTCHEM.2023.101568
18. Raftopoulos KN, Pielichowski K (2016) Segmental dynamics in hybrid polymer/POSS nanomaterials. Prog Polym Sci 52:136–187
19. Lichtenhan JD, Pielichowski K, Blanco I (2019) POSS-Based Polymers. Polym 11:1727. https://doi.org/10.3390/POLYM11101727
20. Liu C, Chiang B, Lewin Mejia D et al (2019) Mammary fibroblasts remodel fibrillar collagen microstructure in a biomimetic nanocomposite hydrogel. Acta Biomater 83:221–232. https://doi.org/10.1016/J.ACTBIO.2018.11.010
21. Pu W, Jiang F, Chen P, Wei B (2017) A POSS based hydrogel with mechanical robustness, cohesiveness and a rapid self-healing ability by electrostatic interaction. Soft Matter 13:5645–5648. https://doi.org/10.1039/C7SM01492A
22. Moshkbar H, Arsalani N, Saleh Ghadimi L (2019) Synthesis of Chitosan/Gelatin granule containing amine derivated octa(ammonium chloride) substituted Polyhedral Oligomeric Silsesquioxane and investigating its application as a drug carrier. Int J Polym Mater Polym Biomater 68:836–843. https://doi.org/10.1080/00914037.2018.1517345
23. Lian X, Shi D, Ma J et al (2018) Peptide dendrimer-crosslinked inorganic-organic hybrid supramolecular hydrogel for efficient anti-biofouling. Chin Chem Lett 29:501–504. https://doi.org/10.1016/J.CCLET.2017.08.014
24. Wang X, Wang J, Yang Y et al (2017) Fabrication of multi-stimuli responsive supramolecular hydrogels based on host-guest inclusion complexation of a tadpole-shaped cyclodextrin derivative with the azobenzene dimer. Polym Chem 8:3901–3909. https://doi.org/10.1039/c7py00698e
25. Renò F, Carniato F, Rizzi M et al (2013) POSS/gelatin-polyglutamic acid hydrogel composites: Preparation, biological and mechanical characterization. J Appl Polym Sci 129:699–706. https://doi.org/10.1002/APP.38789
26. Blanco I (2018) The rediscovery of POSS: a molecule rather than a filler. Polym (Basel) 10. https://doi.org/10.3390/polym10080904
27. Liu S, Guo R, Li C et al (2021) POSS hybrid hydrogels: a brief review of synthesis, properties and applications. Eur Polym J 143:110180. https://doi.org/10.1016/J.EURPOLYMJ.2020.110180
28. Liu G, Wu G, Chen J et al (2015) Synthesis and properties of POSS-containing gallic acid-based non-isocyanate polyurethanes coatings. Polym Degrad Stab 121:247–252. https://doi.org/10.1016/j.polymdegradstab.2015.09.013
29. Liu G, Wu G, Chen J, Kong Z (2016) Synthesis, modification and properties of rosin-based non-isocyanate polyurethanes coatings. Prog Org Coatings 101:461–467. https://doi.org/10.1016/j.porgcoat.2016.09.019
30. Blattmann H, Mülhaupt R (2016) Multifunctional POSS cyclic carbonates and Non-isocyanate polyhydroxyurethane hybrid materials. Macromolecules 49:742–751. https://doi.org/10.1021/acs.macromol.5b02560
31. Liu W, Hang G, Mei H et al (2022) Nanocomposites of Polyhydroxyurethane with POSS Microdomains: Synthesis via Non-Isocyanate Approach, Morphologies and Reprocessing Properties. Polymer 14:1331. https://doi.org/10.3390/POLYM14071331
32. Zhao B, Wei K, Wang L, Zheng S (2020) Poly(hydroxyl urethane) s with double Decker silsesquioxanes in the Main Chains: synthesis, shape recovery, and Reprocessing properties. Macromolecules 53:434–444. https://doi.org/10.1021/acs.macromol.9b01976
33. Hu S, Chen X, Bin Rusayyis MA et al (2022) Reprocessable polyhydroxyurethane networks reinforced with reactive polyhedral oligomeric silsesquioxanes (POSS) and exhibiting excellent elevated temperature creep resistance. Polymer 252:124971. https://doi.org/10.1016/J.POLYMER.2022.124971
34. MacInnis CM, Younes GR, Marić M (2022) The effect of polyhedral oligomeric silsesquioxane fillers in non-isocyanate polyurethane hybrid resins. J Appl Polym Sci 139:e53225. https://doi.org/10.1002/APP.53225
35. Zhao H, Zhao SQ, Li Q et al (2020) Fabrication and properties of waterborne thermoplastic polyurethane nanocomposite enhanced by the POSS with low dielectric constants. Polymer 209:122992. https://doi.org/10.1016/J.POLYMER.2020.122992
36. Lee A, Deng Y (2015) Green polyurethane from lignin and soybean oil through non-isocyanate reactions. Eur Polym J 63:67–73. https://doi.org/10.1016/J.EURPOLYMJ.2014.11.023
37. Błażek K, Kasprzyk P, Datta J (2020) Diamine derivatives of dimerized fatty acids and bio-based polyether polyol as sustainable platforms for the synthesis of non-isocyanate polyurethanes. Polymer 205:122768. https://doi.org/10.1016/J.POLYMER.2020.122768
38. Asemani HR, Mannari V (2019) Synthesis and evaluation of non-isocyanate polyurethane polyols for heat-cured thermoset coatings. Prog Org Coatings 131:247–258. https://doi.org/10.1016/j.porgcoat.2019.02.036
39. Shen Z, Zheng L, Song D et al (2022) A Non-Isocyanate Route to Poly(Ether Urethane): Synthesis and Effect of Chemical Structures of Hard Segment. Polym 14:2039. https://doi.org/10.3390/POLYM14102039
40. Gultekin G, Atalay-Oral C, Erkal S et al (2009) Fatty acid-based polyurethane films for wound dressing applications. J Mater Sci Mater Med 20:421–431. https://doi.org/10.1007/s10856-008-3572-5
41. Kotanen S, Wirtanen T, Mahlberg R et al (2023) Cyclic carbonates as building blocks for non-isocyanate polyurethanes. J Appl Polym Sci 140:e53964. https://doi.org/10.1002/APP.53964
42. Błażek K, Beneš H, Walterová Z et al (2021) Synthesis and structural characterization of bio-based bis(cyclic carbonate)s for the preparation of non-isocyanate polyurethanes. Polym Chem 12:1643–1652. https://doi.org/10.1039/D0PY01576H

43. Feldblum ES, Arkin IT (2014) Strength of a bifurcated H bond. Proc Natl Acad Sci 111:4085–4090. https://doi.org/10.1073/pnas.1319827111
44. Brudler R, de Groot HJM, van Liemt WBS et al (1995) FTIR spectroscopy shows weak symmetric hydrogen bonding of the QB carbonyl groups in Rhodobacter sphaeroides R26 reaction centres. FEBS Lett 370:88–92. https://doi.org/10.1016/0014-5793(95)00805-J
45. Li X, Yang M, Shi X et al (2015) Effect of the intramolecular hydrogen bond on the spectral and optical properties in chitosan oligosaccharide. Phys E Low-dimensional Syst Nanostructures 69:237–242. https://doi.org/10.1016/J.PHYSE.2015.01.043
46. Novak U, Grdadolnik J (2021) Infrared spectra of hydrogen bond network in lamellar perfluorocarboxylic acid monohydrates. Spectrochim Acta Part A Mol Biomol Spectrosc 253:119551. https://doi.org/10.1016/J.SAA.2021.119551
47. Hebda E, Bukowczan A, Michałowski S, Pielichowski K (2022) Flexible polyurethane foams reinforced by functionalized polyhedral oligomeric silsesquioxanes: structural characteristics and evaluation of thermal/flammability properties. Polymers (Basel) 14: https://doi.org/10.3390/POLYM14214743
48. Hebda E, Ozimek J, Raftopoulos KN et al (2015) Synthesis and morphology of rigid polyurethane foams with POSS as pendant groups or chemical crosslinks. Polym Adv Technol 26:932–940. https://doi.org/10.1002/pat.3504
49. Zhao H, She W, Shi D et al (2019) Polyurethane/POSS nanocomposites for superior hydrophobicity and high ductility. Compos Part B Eng 177:107441. https://doi.org/10.1016/J.COMPOSITESB.2019.107441
50. Hao T, Liu X, Hu GH et al (2017) Preparation and characterization of polyurethane/POSS hybrid aqueous dispersions from monoamino substituted POSS. Polym Bull 74:517–529. https://doi.org/10.1007/S00289-016-1727-Y
51. Illescas S, Sánchez-Soto M, Milliman H et al (2011) The morphology and properties of melt-mixed polyoxymethylene/monosilanolisobutyl-POSS composites. High Perform Polym 23:457–467. https://doi.org/10.1177/0954008311415301
52. Jiao L, Xiao H, Wang Q, Sun J (2013) Thermal degradation characteristics of rigid polyurethane foam and the volatile products analysis with TG-FTIR-MS. Polym Degrad Stab 98:2687–2696. https://doi.org/10.1016/J.POLYMDEGRADSTAB.2013.09.032
53. Govorčin Bajsić E, Rek V, Agić A (2003) Thermal degradation of polyurethane elastomers: determination of kinetic parameters. J Elastomers Plast 35:311–323. https://doi.org/10.1177/009524403034393
54. Ketata N, Sanglar C, Waton H et al (2005) Thermal degradation of polyurethane Bicomponent systems in controlled atmospheres. Polym Polym Compos 13:1–26. https://doi.org/10.1177/096739110501300101
55. Bukowczan A, Stachak P, Łukaszewska I et al (2023) Pyrolysis and thermal degradation studies of non-isocyanate polyurethanes modified by polyhedral oligomeric silsesquioxanes. Thermochim Acta 723:179484. https://doi.org/10.1016/J.TCA.2023.179484
56. Parcheta-Szwindowska P, Rohde K, Datta J (2022) Bio-derived polyurethanes obtained by non-isocyanate route using polyol-based bis(cyclic carbonate)s-studies on thermal decomposition behavior. 147:13329–13339. https://doi.org/10.1007/s10973-022-11679-9
57. Simon J, Barla F, Kelemen-Haller A et al (1988) Thermal stability of polyurethanes. Chromatographia 25:99–106. https://doi.org/10.1007/BF02259024
58. Dannoux A, Esnouf S, Amekraz B et al (2008) Degradation mechanism of poly(ether-urethane) Estane® induced by high-energy radiation. II. Oxidation effects. J Polym Sci Part B Polym Phys 46:861–878. https://doi.org/10.1002/POLB.21419
59. Boisaubert P, Kébir N, Schuller AS, Burel F (2022) Polyurethane coatings from formulations with low isocyanate content using a transurethane polycondensation route. Polymer 240:124522. https://doi.org/10.1016/J.POLYMER.2022.124522
60. Reinerte S, Avotina L, Zarins A et al (2020) TG/DTA-FTIR as a method for analysis of tall oil based rigid polyurethane foam decomposition gaseous products in a low oxygen environment. Polym Degrad Stab 180:109313. https://doi.org/10.1016/J.POLYMDEGRADSTAB.2020.109313
61. Pan R, Shanks R, Kong I et al (2014) Trisilanolisobutyl POSS/polyurethane hybrid composites: preparation, WAXS and thermal properties. Polym Bull 71:2453–2464. https://doi.org/10.1007/s00289-014-1201-7
62. Członka S, Strączkowska A, Strzelec K et al (2019) Composites of rigid polyurethane foams reinforced with POSS. Polymers (Basel) 11. https://doi.org/10.3390/polym11020336
63. Pagacz J, Hebda E, Michałowski S et al (2016) Polyurethane foams chemically reinforced with POSS—Thermal degradation studies. Thermochim Acta 642:95–104. https://doi.org/10.1016/J.TCA.2016.09.006
64. Markovic E, Nguyen K, Clarke S et al (2013) Synthesis of POSS–polyurethane hybrids using octakis(m-isoprenyl-α,α′-dimethylbenzylisocyanato dimethylsiloxy) octasilsesquioxane (Q8M8TMI) as a crosslinking agent. J Polym Sci Part A Polym Chem 51:5038–5045. https://doi.org/10.1002/POLA.26934
65. Zhu G-L, Han D, Yuan Y et al (2018) Improving Damping properties and Thermal Stability of Epoxy/Polyurethane grafted Copolymer by adding Glycidyl POSS. Chinese J Polym Sci 36:1297–1302. https://doi.org/10.1007/s10118-018-2145-4
66. Immergut EH, Mark HF (1965) Principles of plasticization. Adv Chem 48:1–26. https://doi.org/10.1021/BA-1965-0048.CH001
67. Dintcheva NT, Morici E, Arrigo R et al (2012) Structure-properties relationships of polyhedral oligomeric silsesquioxane (POSS) filled PS nanocomposites. eXPRESS Polym Lett 6:561–571. https://doi.org/10.3144/expresspolymlett.2012.59
68. Young WW, Saez JP, Katsumata R (2021) Rationalizing the Composition Dependence of Glass Transition Temperatures in Amorphous Polymer/POSS composites. 10:59. https://doi.org/10.1021/acsmacrolett.1c00597
69. Brostow W, Chiu R, Kalogeras IM, Vassilikou-Dova A (2008) Prediction of glass transition temperatures: binary blends and copolymers. Mater Lett 62:3152–3155. https://doi.org/10.1016/j.matlet.2008.02.008
70. Combarro Palacios I, Olsson C, Kamma-Lorger CS et al (2019) Motions of water and solutes - slaving versus plasticization phenomena. J Chem Phys 150:124902. https://doi.org/10.1063/1.5030064
71. Raftopoulos KN, Hebda E, Grzybowska A et al (2020) PEG-POSS Star molecules blended in polyurethane with flexible hard segments: morphology and Dynamics. Molecules 26:99. https://doi.org/10.3390/molecules26010099
72. Hao N, Böhning M, Goering H, Schönhals A (2007) Nanocomposites of polyhedral oligomeric phenethylsilsesquioxanes and poly(bisphenol A carbonate) as investigated by dielectric spectroscopy. Macromolecules 40:2955–2964. https://doi.org/10.1021/MA070036C
73. Di Lisio V, Stavropoulou VM, Cangialosi D (2023) Physical aging in molecular glasses beyond the α relaxation. J Chem Phys 159:64505. https://doi.org/10.1063/5.0157994/2905845
74. Raftopoulos KN, Pandis C, Apekis L et al (2010) Polyurethane-POSS hybrids: molecular dynamics studies. Polymer 51:709–718. https://doi.org/10.1016/j.polymer.2009.11.067
75. Sargsyan A, Tonoyan A, Davtyan S, Schick C (2007) The amount of immobilized polymer in PMMA SiO2 nanocomposites determined from calorimetric data. Eur Polym J 43:3113–3127. https://doi.org/10.1016/J.EURPOLYMJ.2007.05.011
76. McAninch IM, Palmese GR, Lenhart JL, La Scala JJ (2015) DMA testing of epoxy resins: the importance of dimensions. Polym Eng Sci 55:2761–2774. https://doi.org/10.1002/PEN.24167

77. Ayandele E, Sarkar B, Alexandridis P (2012) Polyhedral Oligomeric Silsesquioxane (POSS)-Containing polymer nanocomposites. Nanomaterials 2:445–475. https://doi.org/10.3390/nano2040445
78. Jiang Y, Ding D, Zhao S et al (2018) Renewable thermoset polymers based on lignin and carbohydrate derived monomers. Green Chem 20:1131–1138. https://doi.org/10.1039/C7GC03552G
79. Seyler R (1994) Assignemnt of the glass transition, STP 1249. ASTM International, Philadelphia
80. Stark W (2013) Investigation of the curing behaviour of carbon fibre epoxy prepreg by dynamic mechanical analysis DMA. Polym Test 32:231–239. https://doi.org/10.1016/J.POLYMERTESTING.2012.11.004
81. Koutsoumpis S, Ozimek J, Raftopoulos KN et al (2018) Polyurethanes with POSS pendent on flexible hard segments: morphology and glass transition. Polymer 147:225–236. https://doi.org/10.1016/j.polymer.2018.06.012
82. Zhao S, Abu-Omar MM (2016) Renewable epoxy networks derived from lignin-based monomers: Effect of cross-linking density. ACS Sustain Chem Eng 4:6082–6089. https://doi.org/10.1021/ACSSUSCHEMENG.6B01446
83. Hill LW (1997) Calculation of crosslink density in short chain networks. Prog Org Coatings 31:235–243. https://doi.org/10.1016/S0300-9440(97)00081-7
84. Vishal Gupta N, Shivakumar HG (2012) Investigation of swelling Behavior and Mechanical properties of a pH-Sensitive Superporous Hydrogel Composite. Iran J Pharm Res IJPR 11:481
85. Zhang K, Feng W, Jin C (2020) Protocol efficiently measuring the swelling rate of hydrogels. MethodsX 7:100779. https://doi.org/10.1016/J.MEX.2019.100779
86. Shen J, Li H, Lu C et al (2018) Hydrolytically degradable POSS-PEG hybrid hydrogels prepared in aqueous phase with tunable mechanical properties, swelling ratio and degradation rate. React Funct Polym 123:91–96. https://doi.org/10.1016/J.REACTFUNCTPOLYM.2017.12.008
87. Zhang X, Liu B, Feng W et al (2022) Fully physically crosslinked POSS-based hydrogel with low swelling, high stretchable, self-healing, and conductive properties for human motion sensing. https://doi.org/10.1016/j.colsurfa.2022.130016
88. Seera SDK, Kundu D, Banerjee T (2020) Physical and chemical crosslinked microcrystalline cellulose-polyvinyl alcohol hydrogel: freeze–thaw mediated synthesis, characterization and in vitro delivery of 5-fluorouracil. Cellulose 27:6521–6535. https://doi.org/10.1007/s10570-020-03249-9
89. Sinh Vo T, Thi Bich Chau Vo T, Tien Tran T, Duy Pham N (2021) Enhancement of water absorption capacity and compressibility of hydrogel sponges prepared from gelatin/chitosan matrix with different polyols. https://doi.org/10.1016/j.pnsc.2021.10.001
90. Abdallah AM (2019) The effect of hydrogel particle size on water retention properties and availability under water stress. Orig Res Artic. https://doi.org/10.1016/j.iswcr.2019.05.001
91. Ostroha J, Pong M, Lowman A, Dan N (2004) Controlling the collapse/swelling transition in charged hydrogels. Biomaterials 25:4345–4353. https://doi.org/10.1016/J.BIOMATERIALS.2003.11.019
92. Wang DK, Varanasi S, Strounina E et al (2014). Synthesis and characterization of a POSS-PEG macromonomer and POSS-PEG-PLA hydrogels for periodontal applications. https://doi.org/10.1021/bm401728p